Rapid Communications

Counter-thermal flow of holes in high-mobility $LaNiO_3$ thin films

Changjiang Liu,[1] Friederike Wrobel,[1,2] Jason D. Hoffman,[3] Deshun Hong,[1]
John E. Pearson,[1] Eva Benckiser,[2] and Anand Bhattacharya[1,*]
[1]*Materials Science Division, Argonne National Laboratory, Lemont, Illinois 60439, USA*
[2]*Max Planck Institute for Solid State Research, Heisenbergstrasse 1, 70569 Stuttgart, Germany*
[3]*Department of Physics, Harvard University, Cambridge, Massachusetts 02138, USA*

(Received 5 November 2018; published 22 January 2019)

Measurements of electronic structure and theoretical models indicate that the Fermi surface of $LaNiO_3$ (LNO) is predominantly holelike, with a small electron pocket. However, measurements of the Hall and Seebeck effects yield nominally opposite signs for the dominant charge carrier type, making charge transport in LNO puzzling. Here, we combine measurements of the Hall, Seebeck, and Nernst coefficients in high-mobility epitaxial LNO thin films, and resolve this puzzle by demonstrating that the negative Seebeck coefficient is generated by the diffusion of holes from cold to hot regions of LNO. We further examine this counter-thermal flow of holes by measuring the evolution of the Nernst coefficient from the diffusive to the ballistic regime, where the suppression of energy-dependent scattering leads to a reversal of the flow of holes.

DOI: 10.1103/PhysRevB.99.041114

The rare-earth perovskite nickelates $ReNiO_3$ have been studied extensively over the past several decades. Within this family, $LaNiO_3$ (LNO) is of particular interest as the only one that does not undergo a metal-insulator transition, remaining metallic down to the lowest temperatures [1]. It is believed that in LNO [2], straighter Ni-O-Ni bonds increase the overlap between the $3d$ Ni^{3+} e_g and O^{2-} $2p$ orbitals [3], enhancing metallicity. Calculations of the electronic structure of LNO find a small electron pocket near the Γ point of the Brillouin zone, with a large hole Fermi surface around the R point [4,5]. This was confirmed experimentally by angle-resolved photoemission spectroscopy (ARPES) measurements, which also found an enhanced effective mass for electrons but not for holes [6–9]. X-ray spectroscopies on $ReNiO_3$ have also found an abundance of holes on oxygen in this class of materials [10]. These considerations suggest that holes should play a dominant role in charge transport in LNO. However, in measurements of the Hall effect [11–13] and thermoelectric power [14–17], one obtains nominally opposite signs of charge carrier type. This discrepancy is often attributed to complications of the Fermi surface with no clear explanation or experimental resolution.

Here, we use measurements of the Nernst effect, together with the Hall and Seebeck effects to investigate the transport properties of LNO. The Nernst effect is a phenomenon in which a transverse voltage develops in a material subject to a longitudinal temperature gradient in a perpendicular magnetic field. Unlike the electric field in Hall measurements, a thermal gradient can drive both electrons and holes in the same direction, producing a nonzero transverse voltage even in an electron-hole compensated system [18]. In addition, the Nernst effect is sensitive to the energy dependence of the scattering rate, electronic reconstructions [19,20], Berry curvature in momentum space [21,22], and quasiparticle excitations in superconductors [23]. It is thus a useful probe to study materials of contemporary interest, such as topological semimetals [24], unconventional superconductors [25,26], and correlated electronic systems. In addition to shedding light on the role of electrons and holes in the nickelates, the Nernst effect may also be sensitive to electronic reconstructions arising as a result of magnetism that has been reported in LNO [27] and in LNO-based superlattices [28].

The LNO films were grown on (001)-oriented $(LaAlO)_3(Sr_2TaAlO_6)_{0.7}$ (LSAT) substrates by ozone-assisted molecular beam epitaxy (MBE). A detailed description on the sample growth is presented in the Supplemental Material [29]. To investigate the electric transport properties, we performed temperature-dependent measurements of the longitudinal resistivity (ρ_{xx}) and transverse Hall resistance. Figure 1(a) shows ρ_{xx} measured on two samples of thickness 80 and 25 unit cells (UC), respectively. At $T = 2$ K, for each sample the resistivity $\rho_{2\,\mathrm{K}}$ is less than 10 $\mu\Omega$ cm with a residual resistivity ratio (RRR) $\rho_{300\,\mathrm{K}}/\rho_{2\,\mathrm{K}}$ greater than 11. This RRR is among the highest reported for LNO films [13,30], suggesting that our samples are well oxygenated, since it has been shown that the resistivity of LNO is very sensitive to oxygen-deficiency-induced defects [16,31]. The Hall effect was measured up to 9 T at different temperatures. The results are shown in Fig. 1(b) for the 80-UC sample. Over the entire field range, the Hall response is essentially linear with nondiscernible higher-order terms, which supports a dominant single band in transport. The sign of the Hall coefficient R_H is positive, suggesting predominantly holelike charge carriers, in agreement with previous studies [11,32]. Despite the fact that LNO is a metal, we observed an increase in R_H by about a factor of 3 upon cooling, which is shown in Figs. 1(b) and 1(c). Specifically, R_H increases slowly in the temperature range from $T = 300$ K to about 110 K, while the pace becomes more rapid for $T \lesssim 110$ K. Previous

*anand@anl.gov

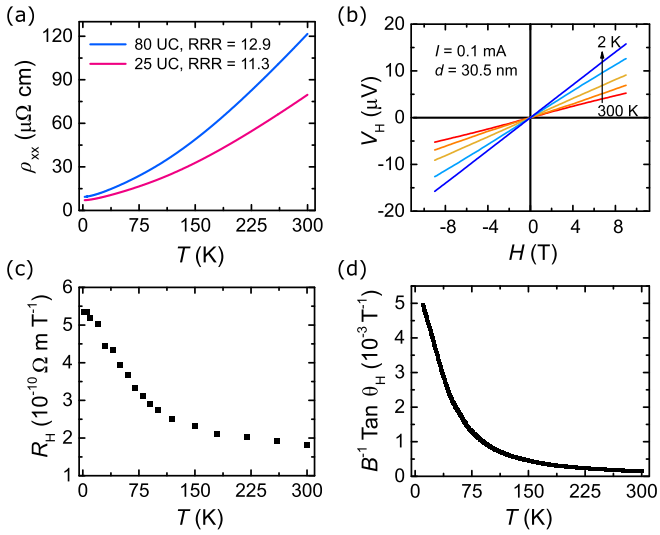

FIG. 1. Electric transport measurements. (a) Temperature dependence of the longitudinal resistivity. (b) Hall voltage measured as a function of magnetic field at different temperatures. The sample has 80 unit cells with a thickness of about 30.5 nm. (c) Temperature dependence of the Hall resistance. (d) Temperature dependence of the Hall angle.

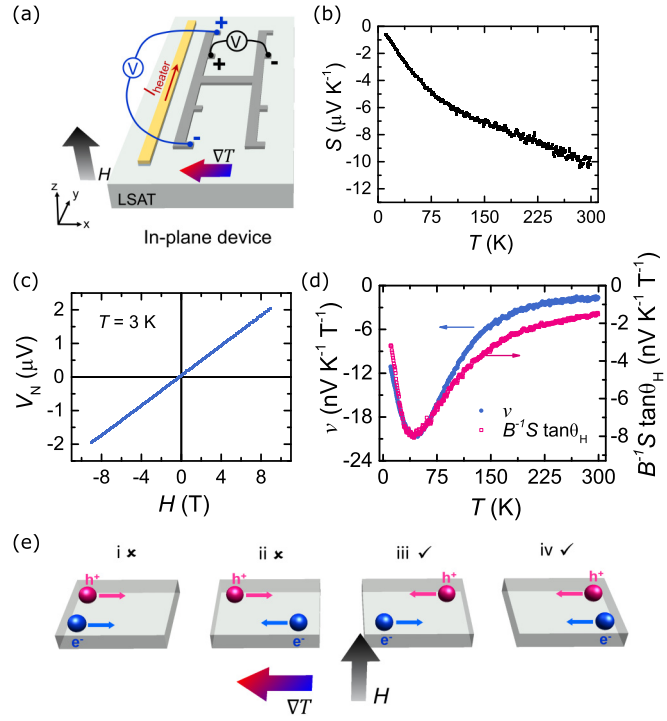

FIG. 2. Device structure and measurement geometry, Seebeck and Nernst results, and illustration of charge transport by both holes and electrons. (a) Schematic of device structures. Heater current flowing in the Au wire is indicated by a red arrow. H is the applied magnetic field. Measurements of the Seebeck and Nernst voltage are illustrated in blue and black, respectively. The corresponding signs of the signal are indicated by the plus/minus symbols. (b) Temperature dependence of the measured Seebeck coefficient S. (c) Nernst voltage measured as a function of magnetic field at $T = 3$ K. (d) Temperature dependence of the measured Nernst coefficient (blue, left axis) and the product of Seebeck coefficient and Hall angle (red, right axis). (e) Four different scenarios for the diffusion of holes (red) and electrons (blue) under a temperature gradient. Only the last two are allowed based on the signs of Nernst and Seebeck measurements.

studies on LNO have also observed an increase of $R_{\rm H}$ with decreasing temperature [11–13], though the magnitude of the overall increase is less pronounced than in our samples. Such temperature-dependent behavior of $R_{\rm H}$ may point to large anisotropic scatterings about the Fermi surface [33], similar to those observed in cuprates [34], and discussed in the context of nickelates [12]. It could also be caused by the opening of a pseudogap as suggested in tunneling measurements on LNO films [35]. Using the measured ρ_{xx} and $R_{\rm H}$, we obtained the Hall angle (θ_H) and plot $B^{-1}\tan\theta_{\rm H}$ (B is the magnetic field in tesla) in Fig. 1(d). We find that $\tan\theta_{\rm H} \ll 1$ at the magnetic fields used in this study, and in the single-band limit this implies $\omega_c\tau \ll 1$, where ω_c is the cyclotron frequency and τ is the momentum relaxation time.

Next, we performed Seebeck and Nernst effect measurements. A schematic of the device and measurement geometry is shown in Fig. 2(a). On-chip heating was achieved by passing an electric current through a 10-μm-wide and 50-nm-thick Au wire, which produces a temperature gradient in the sample plane. There are two parallel 10-μm-wide × 800-μm-long LNO strips connected by a bridging LNO strip of 50-μm width × 250-μm length in the middle. The bridging LNO strip serves as a channel for measuring the Seebeck coefficient. Each of the long parallel LNO strips has four contacts for measuring changes in resistance, serving as thermometers. The Nernst signal was obtained by measuring the voltage along the long LNO strip (y direction, the one closer to the heater), with magnetic field applied along the z direction. During measurements, the heater current was modulated at $f = 3$ Hz, and a lock-in amplifier was used to measure the thermoelectric response at $2f$.

Figure 2(b) shows the temperature dependence of the measured Seebeck coefficient S, which is negative over the entire temperature range, in agreement with previous studies on LNO [12,16]. A positive value of $R_{\rm H}$ together with a negative value of S have also been seen in the metallic phase of other nickelates [36–38]. The negative sign of S was interpreted as a response of electronlike charge carriers. However, it is known from the Mott formula that S depends on the derivative of conductivity with respect to energy at the Fermi level [39], which can be either positive or negative. This dependence of the sign of S implies that for a given charge carrier type, the diffusion can be either from a hot to a cold region or vice versa depending on the particular material. However, this point is often missed. In the following, by using Nernst effect measurements we determine that a counter-thermal flow of holes is mainly responsible for the negative Seebeck coefficient in LNO.

Figure 2(c) shows the Nernst voltage measured as a function of magnetic field at $T = 3$ K. The Nernst voltage shows a linear field dependence, and the corresponding sign is indicated by the blue plus/minus symbols in Fig. 2(a). The Nernst response was linear in applied magnetic field over the full

temperature range (see Supplemental Material [29]). In this measurement, ∇T is along the negative x direction (points to the heater) and the magnetic field is along the positive z direction. According to the "vortex" convention [18], the sign of the measured Nernst coefficient ν is negative. The temperature dependence of ν is shown in Fig. 2(d). Because of the uncertainty in determining ∇T in the 10-μm strip, the accuracy of ν is only of the order unity [29].

Intuitively, the Nernst voltage is due to the Lorentz force acting on a charge current that is driven by a longitudinal ∇T. However, if the system has only a single band and τ has no energy dependence, the Nernst signal would be zero even though S is nonzero. This is because in open circuit conditions, there is no net longitudinal current flow as the current driven by the thermal driving force is exactly canceled by an opposing current driven by the Seebeck electric field. In a perpendicular magnetic field, the transverse voltages resulting from these two opposing currents also cancel, and there is no Nernst signal. This effect is known as Sondheimer cancellation [25,40]. However, the carriers that participate in the two counter-flowing currents actually originate from different parts of the energy spectrum [41]. Thus if τ is energy dependent, the transverse flows arising from Lorentz forces no longer cancel and a finite Nernst signal obtains. The general expression for the Nernst coefficient is given by [18,25]

$$\nu = \left(\frac{S}{B}\right)[\tan(\theta_\alpha) - \tan(\theta_{\rm H})] = \frac{\pi^2}{3}\frac{k_{\rm B}^2 T}{qB}\left.\frac{\partial \tan(\theta_{\rm H})}{\partial \varepsilon}\right|_{\varepsilon=\varepsilon_{\rm F}}, \tag{1}$$

where θ_α is the "Hall" angle for thermally driven carriers, $k_{\rm B}$ is the Boltzmann constant, T is the temperature, and q is the electric charge. For the case of a dominant single band, $\tan\theta_{\rm H} \approx \omega_c\tau(\varepsilon) = \frac{qB}{m^*}\tau(\varepsilon)$. If we assume a constant effective mass m^* [18,19],

$$\nu = \frac{\pi^2}{3}\frac{k_{\rm B}^2 T}{m^*}\left.\frac{\partial \tau}{\partial \varepsilon}\right|_{\varepsilon=\varepsilon_{\rm F}}, \tag{2}$$

where $\varepsilon_{\rm F}$ is the Fermi energy. From Eq. (2), we see that the sign of ν does not depend on the type of charge carrier but rather on $\frac{\partial\tau}{\partial\varepsilon}|_{\varepsilon_{\rm F}}$. From our measurement, the Nernst coefficient ν of LNO is negative which suggests that $\frac{\partial\tau}{\partial\varepsilon}|_{\varepsilon_{\rm F}} < 0$.

We now examine whether a single-band picture is appropriate for LNO. We consider a model with two simplifying assumptions. Generally, τ varies smoothly about $\varepsilon_{\rm F}$ for $k_{\rm B}T \ll \varepsilon_{\rm F}$ [18]. Specifically, if we assume that $\tau(\varepsilon) \propto \varepsilon^r$ [42], then the Nernst coefficient can be written as

$$\nu = \frac{\pi^2}{3}\frac{k_{\rm B}^2 T}{m^*}\frac{\tau_{\rm F}}{\varepsilon_{\rm F}} r. \tag{3}$$

If we make the additional assumption that the density of states also follows a power law $D(\varepsilon) \propto \varepsilon^w$, then the Seebeck coefficient in a single band picture may be written as

$$S = \frac{\pi^2 k_{\rm B}^2 T}{3q}\left.\frac{\partial[\ln(\sigma)]}{\partial\varepsilon}\right|_{\varepsilon=\varepsilon_{\rm F}} = \frac{\pi^2 k_{\rm B}^2 T}{3q\varepsilon_{\rm F}}(1+w+r), \tag{4}$$

where $\sigma = \frac{ne^2\tau}{m^*}$ is the Drude conductivity [42]. We can now rewrite ν in terms of the Seebeck coefficient and Hall angle as

$$\nu = \frac{r}{1+w+r} B^{-1} S \tan\theta_{\rm H}. \tag{5}$$

We expect $\frac{r}{1+w+r}$ to be of order unity. As seen in Fig. 2(d), the Nernst coefficient ν of LNO increases as temperature decreases, reaching a maximum at $T \sim 50$ K. At lower T, ν approaches zero. The overall $\nu(T)$ dependence is largely captured by the product of $B^{-1}S\tan\theta_{\rm H}$, as shown in Fig. 2(d). Furthermore, the magnitudes of the two quantities are comparable, which indicates that a single-band picture may indeed be a good approximation for LNO. We note that $B^{-1}S\tan\theta_{\rm H}$ would be significantly suppressed in comparison to ν for a strongly compensated system comprising electrons and holes [18] (if compensation is exact, $S = 0$ while ν is large). However, our results do not rule out the possibility of multiple hole bands that may be present in nickelates [43]. Our data also suggest that the main contribution to the Nernst signal comes from deflections of moving holes by the external magnetic field, with no appreciable anomalous Nernst signals due to possible charge/magnetic ordering in LNO.

We now combine the Seebeck and Nernst measurements to address how charge carriers move in LNO. We include transport from both hole and electron bands, though a single band may be sufficient according to the discussion above. There are a total of four scenarios which are illustrated in Fig. 2(d). In each case, the direction of $\nabla_x T$ is the same as in Fig. 2(a), i.e., the left-hand side is at a higher temperature, and the magnetic field is along positive z direction. In scenario (i), both holes (red) and electrons (blue) move from the left to right. This situation is not allowed based on the sign of the measured Nernst voltage, and the right-hand rule for Lorentz forces acting on charge carriers. Scenario (ii) is also not permitted because it would produce a positive Seebeck coefficient. Scenario (iii) satisfies the negative sign of the Seebeck coefficient, however, we need $|\alpha^{\rm h}_{yx}| > |\alpha^{\rm e}_{yx}|$ in order to produce the correct sign of the Nernst signal. Here, $\alpha^{\rm h(e)}$ is the thermoelectric conductivity tensor of holes (h) and electrons (e), defined as $j_x^{\rm h(e)} = -\alpha_{xx}^{\rm h(e)}\nabla_x T$ and $j_y^{\rm h(e)} = -\alpha_{yx}^{\rm h(e)}\nabla_x T$. The last scenario (iv) gets the correct sign for the Nernst voltage, however, it requires $|\alpha^{\rm h}_{xx}| > |\alpha^{\rm e}_{xx}|$ in order to get a negative Seebeck coefficient. From the analysis, we see that the thermoelectric conductivity of holes has to be larger than that of electrons, and that holes have to diffuse from the cold region to the hot region. We note that the predominant role of holes is consistent with the positive Hall coefficient as shown in Fig. 1.

According to Eq. (4), for a given charge carrier type, the direction of diffusive motion is determined by the values of w and r. If $\frac{\partial\sigma}{\partial\varepsilon}|_{\varepsilon_{\rm F}} < 0$, or $w + r < -1$, charge carriers will diffuse from cold regions to hot regions. Previous calculations of the electronic band structure of LNO and ARPES experiments have shown that $\frac{\partial D(\varepsilon)}{\partial\varepsilon}|_{\varepsilon_{\rm F}}$ of LNO (or w in our simplified model) is indeed negative [44–46]. Our Nernst measurement has also shown that $\frac{\partial\tau}{\partial\varepsilon}|_{\varepsilon_{\rm F}} < 0$ (i.e., $r < 0$). This was also reported in optical studies on LNO films [47,48], where it was found that the relaxation rate $1/\tau$ increases strongly with energy at low energies (<50 meV), which was attributed

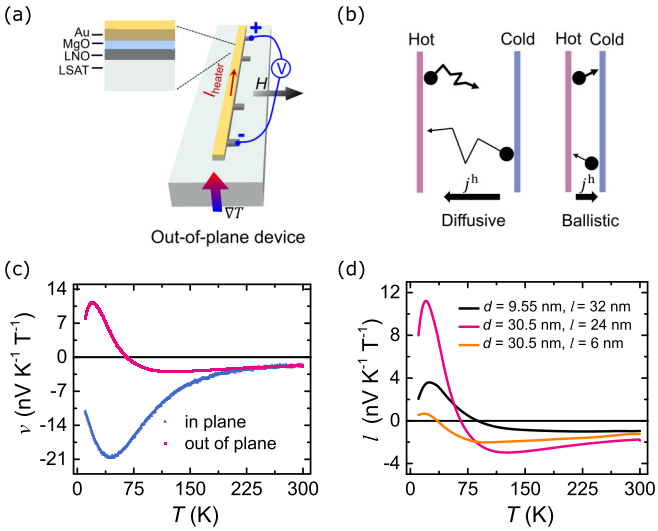

FIG. 3. Out-of-plane Nernst device, illustration of diffusive and ballistic transports, and measurement results. (a) Device structure of the out-of-plane device and measurement geometry. (b) Illustration of the diffusive and ballistic thermal transport of holes in LNO. Thicker arrows represent higher velocity. (c) Temperature dependence of Nernst coefficients measured in the out-of-plane geometry (red) in contrast to that obtained with the temperature gradient in the sample plane (blue). (d) Nernst coefficients measured on samples with different thicknesses and mobilities which are represented by the mean free paths at $T = 10$ K.

to strong electronic correlations [48]. These considerations imply that the decrease of $D(\varepsilon)$ and $\tau(\varepsilon)$ with energy at ε_F are the main mechanisms for holes diffusing in the opposite way in LNO to that in a free-electron system.

The discussions above are based on Boltzmann transport involving diffusive processes, which do not apply in the ballistic regime where momentum relaxation and $\frac{\partial\tau}{\partial\varepsilon}|_{\varepsilon_F}$ play no role. This should give rise to qualitative changes in hole transport between the diffusive and ballistic regimes. Ballistic transport in our high-mobility LNO films can be achieved in the out-of-plane direction at low temperatures. The mean free path l can be estimated by $l = v_F\tau = \frac{\hbar k_F}{m^*}\frac{m^*}{e^2 n\rho_{xx}}$, where v_F is the Fermi velocity, k_F is the Fermi wave vector, and e is the magnitude of the elementary charge. Here, we assume a single band to calculate the carrier concentration n, and a spherical hole Fermi surface. A plot of l over the whole temperature range is shown in the Supplemental Material [29]. For one of the thicker films, at $T = 10$ K, $l \sim 24$ nm which is comparable to thickness $d = 30.5$ nm, approaching ballistic transport in the out-of-plane direction.

To investigate this further, we fabricated devices [Fig. 3(a)] with ∇T in the out-of-plane direction. Figure 3(b) schematically shows the effect of an energy-dependent scattering rate. In the diffusive regime, holes from the hot side carry higher energy (indicated by thicker lines), however, they diffuse slower than those from the cold side. This is presumably because higher-energy holes experience significantly higher scattering rates than those of low energy. On the contrary, when d is comparable to l as shown in the right panel of Fig. 3(b), high-energy holes can traverse the film more quickly because no scattering occurs during the process. As a consequence, the net flow of holes is *opposite* to that in the diffusive regime in this scenario. Experimentally, it is nearly impossible to measure a thermoelectric voltage in the out-of-plane direction in a thin film. However, the Nernst effect provides a unique probe of this effect by generating a transverse (in-plane) voltage from the flow of carriers in the out-of-plane direction [Fig. 3(a)] using an in-plane magnetic field.

Figure 3(c) shows ν measured on the out-of-plane device (red curve) compared to that obtained on the in-plane device (blue curve). For $T \gtrsim 210$ K, ν in the two cases are nearly the same. As T decreases, the out-of-plane measurement starts to deviate from the in-plane one, eventually changing sign. To examine whether this behavior is due to a crossover from diffusive to ballistic transport, we measured the Nernst effect on samples with different mobilities (or l) and thicknesses d. As seen in Fig. 3(d), on different samples the values of T_0 where ν changes sign are different. In the diffusive limit at higher T, $\frac{l}{d} \ll 1$ (0.017 and 0.032 for the thicker samples at 300 K). As T decreases, the thinner sample with longer l shows a higher T_0 (black data), while the thicker sample with shorter l has a much lower T_0. In addition, we found that at the temperature where ν reaches a minimum, the corresponding $\frac{l}{d}$ values range from 0.08 to 0.18 [29]. These observations imply that a crossover from diffusive to ballistic transport begins to occur when $\frac{l}{d} \sim 0.1$, and that upon further increase in $\frac{l}{d}$ a reversal of the flow of holes takes place, eventually leading to a sign change in the Nernst signal at T_0.

In conclusion, by combining measurements of the Nernst, Seebeck, and Hall effects, we have determined that the counter-thermal diffusion of holes explains electrical and thermoelectric transport in LNO, resolving a long-standing conundrum where the Hall and Seebeck measurements gave apparently contradictory results. We further demonstrated that this counter-thermal flow of holes breaks down upon crossing over from the diffusive to the ballistic regime, leading also to a sign change in the Nernst coefficient. We point out that the negative value of $\frac{\partial\tau}{\partial\varepsilon}|_{\varepsilon_F}$ is crucial for understanding these transport phenomena in LNO. The reason for the increase in R_H with decreasing temperature remains an open question. Further theoretical work is required to understand the underlying mechanisms, which will help pave the way for designing oxide thermoelectrics [49] and will improve our understanding of transport in correlated materials.

All work at Argonne was supported by the U.S. Department of Energy, Office of Science, Basic Energy Sciences, Materials Sciences and Engineering Division including support for F.W. via the Center for Predictive Simulation of Functional Materials. The use of facilities at the Center for Nanoscale Materials, an Office of Science user facility, was supported by the U.S. Department of Energy, Basic Energy Sciences under Contract No. DE-AC02-06CH11357. The 25-UC film shown in Figs. 1(a) and 3(d) was grown at Max Planck Institute for Solid State Research, Stuttgart with the help of Dr. Gennady Logvenov. F.W. and E.B. thank the Deutsche Forschungsgemeinschaft (DFG) for financial support under Grant No. TRR 80, Projects No. G1. We thank Michael Norman and Bernhard Keimer for discussions.

[1] J. B. Torrance, P. Lacorre, A. I. Nazzal, E. J. Ansaldo, and C. Niedermayer, Phys. Rev. B **45**, 8209 (1992).

[2] S. J. May, J.-W. Kim, J. M. Rondinelli, E. Karapetrova, N. A. Spaldin, A. Bhattacharya, and P. J. Ryan, Phys. Rev. B **82**, 014110 (2010).

[3] S. Middey, J. Chakhalian, P. Mahadevan, J. Freeland, A. Millis, and D. Sarma, Annu. Rev. Mater. Res. **46**, 305 (2016).

[4] N. Hamada, J. Phys. Chem. Solids **54**, 1157 (1993).

[5] S. B. Lee, R. Chen, and L. Balents, Phys. Rev. B **84**, 165119 (2011).

[6] R. Eguchi, A. Chainani, M. Taguchi, M. Matsunami, Y. Ishida, K. Horiba, Y. Senba, H. Ohashi, and S. Shin, Phys. Rev. B **79**, 115122 (2009).

[7] E. Sakai, M. Tamamitsu, K. Yoshimatsu, S. Okamoto, K. Horiba, M. Oshima, and H. Kumigashira, Phys. Rev. B **87**, 075132 (2013).

[8] P. D. C. King, H. I. Wei, Y. F. Nie, M. Uchida, C. Adamo, S. Zhu, X. He, I. Božović, D. G. Schlom, and K. M. Shen, Nat. Nanotechnol. **9**, 443 (2014).

[9] H. K. Yoo, S. I. Hyun, L. Moreschini, H.-D. Kim, Y. J. Chang, C. H. Sohn, D. W. Jeong, S. Sinn, Y. S. Kim, A. Bostwick, E. Rotenberg, J. H. Shim, and T. W. Noh, Sci. Rep. **5**, 8746 (2015).

[10] V. Bisogni, S. Catalano, R. J. Green, M. Gibert, R. Scherwitzl, Y. Huang, V. N. Strocov, P. Zubko, S. Balandeh, J.-M. Triscone, G. Sawatzky, and T. Schmitt, Nat. Commun. **7**, 13017 (2016).

[11] J. Son, P. Moetakef, J. M. LeBeau, D. Ouellette, L. Balents, S. J. Allen, and S. Stemmer, Appl. Phys. Lett. **96**, 062114 (2010).

[12] E. J. Moon, J. M. Rondinelli, N. Prasai, B. A. Gray, M. Kareev, J. Chakhalian, and J. L. Cohn, Phys. Rev. B **85**, 121106 (2012).

[13] F. Wrobel, A. F. Mark, G. Christiani, W. Sigle, H.-U. Habermeier, P. A. van Aken, G. Logvenov, B. Keimer, and E. Benckiser, Appl. Phys. Lett. **110**, 041606 (2017).

[14] K. Rajeev, G. Shivashankar, and A. Raychaudhuri, Solid State Commun. **79**, 591 (1991).

[15] X. Q. Xu, J. L. Peng, Z. Y. Li, H. L. Ju, and R. L. Greene, Phys. Rev. B **48**, 1112 (1993).

[16] N. Gayathri, A. K. Raychaudhuri, X. Q. Xu, J. L. Peng, and R. L. Greene, J. Phys.: Condens. Matter **10**, 1323 (1998).

[17] J.-S. Zhou, L. G. Marshall, and J. B. Goodenough, Phys. Rev. B **89**, 245138 (2014).

[18] K. Behnia, J. Phys.: Condens. Matter **21**, 113101 (2009).

[19] R. Bel, K. Behnia, and H. Berger, Phys. Rev. Lett. **91**, 066602 (2003).

[20] H. Xing, L. Wen, C. Shen, J. He, X. Cai, J. Peng, S. Wang, M. Tian, Z.-A. Xu, W. Ku, Z. Mao, and Y. Liu, Phys. Rev. B **97**, 041113 (2018).

[21] D. Xiao, Y. Yao, Z. Fang, and Q. Niu, Phys. Rev. Lett. **97**, 026603 (2006).

[22] M. Ikhlas, T. Tomita, T. Koretsune, M.-T. Suzuki, D. Nishio-Hamane, R. Arita, Y. Otani, and S. Nakatsuji, Nat. Phys. **13**, 1085 (2017).

[23] K. Behnia and H. Aubin, Rep. Prog. Phys. **79**, 046502 (2016).

[24] T. Liang, Q. Gibson, J. Xiong, M. Hirschberger, S. P. Koduvayur, R. J. Cava, and N. P. Ong, Nat. Commun. **4**, 2696 (2013).

[25] Y. Wang, Z. A. Xu, T. Kakeshita, S. Uchida, S. Ono, Y. Ando, and N. P. Ong, Phys. Rev. B **64**, 224519 (2001).

[26] R. Daou, J. Chang, D. LeBoeuf, O. Cyr-Choinière, F. Laliberté, N. Doiron-Leyraud, B. J. Ramshaw, R. Liang, D. A. Bonn, W. N. Hardy, and L. Taillefer, Nature (London) **463**, 519 (2010).

[27] H. Guo, Z. W. Li, L. Zhao, Z. Hu, C. F. Chang, C.-Y. Kuo, W. Schmidt, A. Piovano, T. W. Pi, O. Sobolev, D. I. Khomskii, L. H. Tjeng, and A. C. Komarek, Nat. Commun. **9**, 43 (2018).

[28] J. D. Hoffman, B. J. Kirby, J. Kwon, G. Fabbris, D. Meyers, J. W. Freeland, I. Martin, O. G. Heinonen, P. Steadman, H. Zhou, C. M. Schlepütz, M. P. M. Dean, S. G. E. te Velthuis, J.-M. Zuo, and A. Bhattacharya, Phys. Rev. X **6**, 041038 (2016).

[29] See Supplemental Material at http://link.aps.org/supplemental/10.1103/PhysRevB.99.041114 for details of film growth, thermal analysis, and transport measurements.

[30] J. Zhang, H. Zheng, Y. Ren, and J. F. Mitchell, Cryst. Growth Des. **17**, 2730 (2017).

[31] D. Misra and T. K. Kundu, Mater. Res. Express **3**, 095701 (2016).

[32] J. Fowlie, M. Gibert, G. Tieri, A. Gloter, J. Íñiguez, A. Filippetti, S. Catalano, S. Gariglio, A. Schober, M. Guennou, J. Kreisel, O. Stéphan, and J.-M. Triscone, Adv. Mater. **29**, 1605197 (2017).

[33] A. Rosch, Phys. Rev. B **62**, 4945 (2000).

[34] M. Abdel-Jawad, M. P. Kennett, L. Balicas, A. Carrington, A. P. Mackenzie, R. H. McKenzie, and N. E. Hussey, Nat. Phys. **2**, 821 (2006).

[35] S. J. Allen, A. J. Hauser, E. Mikheev, J. Y. Zhang, N. E. Moreno, J. Son, D. G. Ouellette, J. Kally, A. Kozhanov, L. Balents, and S. Stemmer, APL Mater. **3**, 062503 (2015).

[36] S. D. Ha, R. Jaramillo, D. M. Silevitch, F. Schoofs, K. Kerman, J. D. Baniecki, and S. Ramanathan, Phys. Rev. B **87**, 125150 (2013).

[37] A. J. Hauser, E. Mikheev, N. E. Moreno, T. A. Cain, J. Hwang, J. Y. Zhang, and S. Stemmer, Appl. Phys. Lett. **103**, 182105 (2013).

[38] S. Catalano, M. Gibert, J. Fowlie, J. Íñiguez, J.-M. Triscone, and J. Kreisel, Rep. Prog. Phys. **81**, 046501 (2018).

[39] N. F. Mott, *Metal-Insulator Transition* (Taylor & Francis, London, 1990).

[40] E. H. Sondheimer, Proc. R. Soc. London, Ser. A **193**, 484 (1948).

[41] For the thermally driven current, the carriers that matter most are from regions above and below the chemical potential, whereas the maximal contribution for the counter-flowing current driven by the "Seebeck" electric field comes from carriers at the chemical potential.

[42] P. Pichanusakorn and P. Bandaru, Mater. Sci. Eng., R **67**, 19 (2010).

[43] H. Li, X. Zhou, T. Nummy, J. Zhang, V. Pardo, W. E. Pickett, J. F. Mitchell, and D. S. Dessau, Nat. Commun. **8**, 704 (2017).

[44] L. Guan, B. Liu, L. Jin, J. Guo, Q. Zhao, Y. Wang, and G. Fu, Solid State Commun. **150**, 2011 (2010).

[45] J. He and C. Franchini, Phys. Rev. B **86**, 235117 (2012).

[46] H. K. Yoo, S. I. Hyun, Y. J. Chang, L. Moreschini, C. H. Sohn, H.-D. Kim, A. Bostwick, E. Rotenberg, J. H. Shim, and T. W. Noh, Phys. Rev. B **93**, 035141 (2016).

[47] D. G. Ouellette, S. B. Lee, J. Son, S. Stemmer, L. Balents, A. J. Millis, and S. J. Allen, Phys. Rev. B **82**, 165112 (2010).

[48] M. K. Stewart, C.-H. Yee, J. Liu, M. Kareev, R. K. Smith, B. C. Chapler, M. Varela, P. J. Ryan, K. Haule, J. Chakhalian, and D. N. Basov, Phys. Rev. B **83**, 075125 (2011).

[49] B. Geisler, A. Blanca-Romero, and R. Pentcheva, Phys. Rev. B **95**, 125301 (2017).